Neutron tomography methods applied to a nickel-based superalloy additive manufacture build

Turner, Richard; Panwisawas, Chinnapat; Lu, Yu; Dhiman, Indu; Basoalto, Hector; Brooks, Jeffery

DOI:
10.1016/j.matlet.2018.07.112

Neutron Tomography Methods applied to a Nickel-based Superalloy Additive Manufacture build

R.P. Turner[1*], C. Panwisawas[1,2], Y. Lu[1], I. Dhiman[3], H.C. Basoalto[1], J.W. Brooks[1]

[1] School of Metallurgy & Materials, University of Birmingham, Birmingham, B15 2TT, UK
[2] Department of Materials, University of Oxford, Oxford, OX5 1PF, UK
[3] Neutron Scattering Division, Oak Ridge National Laboratory, Oak Ridge, Tennessee, 37831, USA
* r.p.turner@bham.ac.uk

Abstract

Selective-laser melting (SLM) is one of the most rapidly developing and promising of all the so-called "Additive Manufacture" routes due to its capability to produce component geometries that would prove impossible using traditional manufacture. A selective-laser melting fabricated cuboid component was built using powder CM247LC, using standard methods, and this was subsequently analysed using neutron tomography methodology to allow for three-dimensional visualisation of the exterior and the interior of the component. The resulting neutron radiographs were processed and analysed for evidence of both porosity and grain boundary segregation within the component.

Keywords: Selective-laser-melting, Attenuation, Porosity, Grain-boundary segregation, CM247LC

1. Introduction

Selective layer melting (SLM) is one of the rapidly increasing manufacturing routes [1] that make up the so-called 'Additive Manufacture' family of manufacturing processes. The manufacture of structural components from Nickel-based superalloys using these developing additive techniques is increasing in popularity as industries such as aerospace and aero-engine sectors are investing in additive manufacture research. As with many powder processing routes, selective laser melting (SLM) can produce highly complex components with an internal structural build that would be impossible to produce using any traditional manufacturing route [2]. SLM offers one of the most precise additive manufacture processes, largely due to its small laser source diameter (approximately 250 μm) and its very small deposition layer thickness (typically 30-50 μm), which therefore offers a much improved surface finish compared to other additive processes [3]. However this does of course come at the expense of slower deposition rates and thus slower build times.

The ease with which a nickel-based superalloy can be successfully fabricated using SLM largely depends upon the composition of the alloy. Whilst some superalloys are relatively easy to form using SLM, these tend to be alloys with a low volume fraction of γ' precipitates [4]. However, the improved creep-life that can be achieved by nickel-based superalloys with a higher volume fraction of γ' precipitate has led to these alloys being preferred for safety-critical components. This work considers SLM fabrication of high content γ' alloys, and demonstrates the use of neutron tomography methods to investigate porosity during the solidification stage and the resultant localised chemical composition within the builds.

2. Material and methods

2.1 SLM fabrication

CM247LC is an example of a larger volume fraction γ' precipitate-forming superalloys which can give improved creep resistance, strength and thus improved in-service life. CM247LC is a Cannon-Muskegon developed variant of the nickel-based superalloy Mar M 247 developed by Martin Marietta Corporation [5]. An SLM-built CM247LC 15mm x 15mm x 30 mm tower was fabricated. The build was then sectioned using EDM wire erosion to cut narrower 7.5 mm x 7.5 mm x 30 mm sub-towers (as shown in Figure 1), to allow sufficient transmission of neutrons through the sample and hence produce a reasonable image. Two opposing corner sub-builds were examined using neutron tomography.

2.2 Neutron Tomography

Neutron tomography is a non-destructive, non-invasive method allowing through-thickness resolution of a sample [6]. The difference in attenuation coefficient of different elements for a cold neutron beam produces variation/contrast in the measured/recorded radiographs on the CCD detector placed in transmission geometry. Neutron tomography methods can reveal the sub-surface structure of a component. Thus, the approach is highly applicable to determine the presence and distribution of sub-surface porosity within the SLM-built structure [7]. The attenuation of a neutron beam for a uniform sample thickness and homogeneous material of a single isotope is given by:

$$I(\lambda) = I_0(\lambda)e^{-\mu(\lambda)\Delta x} \qquad \textit{Equation 1}$$

For I and I_0 the transmitted and incident beam intensity, μ the attenuation coefficient, λ the neutron wavelength and Δx the sample thickness [6]. The attenuation coefficient can be calculated using:

$$\mu(\lambda) = \sigma_t(\lambda)\frac{\rho N_A}{M_{molar}} \qquad \textit{Equation 2}$$

where σ_t is sample cross-sectional area, ρ the density, N_A is Avogadro's constant and M_{molar} is molar mass. Note that neutron attenuation is dependent upon the wavelength of the neutron source [6].

For the experimental set-up, the CG-1D imaging beamline at Oak Ridge National Laboratory, within the High Flux Isotope Reactor (HFIR) facility was used. This tomography system has a line of flight from neutron beam aperture to detector of L=6.59m. The aperture was set to D=4.1mm, thus producing an L/D ratio of ~1600:1. A rotation stage is positioned in between aperture and detector to mount and rotate the sample through 360° and a CCD detector unit [6,8] positioned behind the sample. The cold neutron wavelength ranged from 0.8 to 6 Å, with a peak neutron intensity at 2.6Å ($2.6\text{x}10^{-10}$m), and based upon the chemical composition of the CM247LC superalloy (see Table 1), the material density and the sample thickness, the transmitted beam was predicted to have an intensity of ~$0.135I_0$-$0.225I_0$, depending upon the rotational position of the cuboid sample (the lower transmission corresponding to the beam travelling across a leading diagonal of the cuboid). The sample was rotated at increments of 0.91° to produce 395 images taken through the full 360° rotation of the sample.

An open-beam image (with no sample in the path of the aperture to detector) must be performed prior to the experimental set-up, in order to account for any beam inhomogeneities. Finally, all neutron tomography radiographs taken by the CCD detector are corrected for dark-field which allows the produced image to correct for electronic noise generated by the CCD detector. The tomography data was reconstructed using a software package called OCTOPUS [9].

3. Results & discussion

3.1 Porosity visualisation

The resulting 3D reconstructed data was visualised and analysed using the Avizo software [10] to study sub-surface porosity. The resulting porosity within two opposing corners A and B of the same SLM build revealed significant variations in porosity measurements – see Figure 2.

As is typical of powder processing manufacture, the consolidation of powder particles to form the structural component is of critical importance. Microscale void defects (micro-voids) can form within an SLM formed component at various locations due to one of three principal mechanisms: (a) where the metallic powder has not been heated enough to produce melting of the particle to allow a bonding to the adjacent layer, or alternatively (b) the particle has been heated to above the alloy liquidus temperature but due to the speed of the laser heat source, the time in the molten phase is so brief that the viscous molten particle does not have enough time to "drip" down to fill the voids present across the layer of powder particles due to spherical packing. Finally, (c) a melt-induced porous void can form within the fully molten region of the build due to induced fluid flow or due to superheated material exceeding the vaporisation temperature, which leads to gas bubble formation inside the molten material. Upon solidification, these gas bubbles become trapped.

The so-called lack of fusion pores are of a similar size to the particle diameter, thus would be expected to vary in the range of 15-40 μm. These are of the relevant size to be observed by the typical resolution of neutron tomography methods. The latter melt-induced pores are typically of the order of 1 μm in diameter, and are difficult to observe experimentally using neutrons, and consequently are not considered further in this work.

The significant location-specific variation in the lack-of-fusion porosity measured using this neutron tomography technique when comparing region A and region B of the same SLM sample would strongly suggest an impact upon the property distribution within the component and subsequent in-service performance. In addition including the levels of any manufacture-route induced residual stresses are likely to be modified by the heterogeneous porosity distribution.

3.2 Grain-boundary segregation visualisation

The neutron radiographs were analysed using Azivo software to assess the attenuation of the neutron beam across grains within the build. Figure 2 shows a network of lighter regions indicating lower attenuation and thus a variation in chemical composition close to the grain boundaries. The SLM-built components thus required advanced characterisation methods to determine the chemistry within the grain and within the layered segregation phase close to the grain boundary.

Energy-dispersive spectroscopy (EDX) methods were employed using the Jeol JSM-7000F SEM equipped with an Oxford instruments Inca 300 EDX system. A region of the build close to the base of the component was analysed. A line-scan was performed across the length of a grain including the grain boundary regions (see Figure 3). Chemical analysis of the grain and boundary regions have been calculated from the resulting EDX analysis, and the composition of the scanned domain is given in Table 1. The layered bulk phase close to the grain boundary was approximately 0.5-1 μm in thickness, whereas typically grain boundary complexions measure only a few nm in thickness, thus requiring atom probe techniques to determine [11,12].

The measured chemical composition of this layered phase close to grain boundaries shows increased hafnium and tantalum content, and depleted cobalt and nickel content. Hafnium in particular has been reported to segregate toward the grain boundary within Ni-base superalloys [4,13], thus it is not surprising to find it in higher concentration within this layered bulk phase. A layered bulk phase coincident to the grain boundary has been reported within the literature before [14]. The authors concluded that the presence of the layered phase was connected with complete / incomplete wetting of the grain boundaries, and the associated higher entropy of the liquid compared to solid phase effectively provided a mechanism for a phase transformation. This has been observed for both the Al-Zn [14] and Cu-Co [15] systems.

4. Conclusions

A neutron tomography experiment was conducted upon an SLM-fabricated simple cuboid component, to illustrate the applicability of this technique to non-destructively analyse SLM components. The following conclusions are drawn.

- The measured porosity significantly varied within the two different locations across the width of the SLM component. This porosity variation could potentially have important effects upon location-specific properties and component design.
- A layered bulk phase close to the grain boundaries, hypothesised to be caused by wetting effects, was detected within the SLM-built component. The second phase forms in layers of approximately 0.5-1 µm thickness as determined by EDX analysis.

5. Acknowledgements

This research used resources at the High Flux Isotope Reactor (HFIR), a DOE Office of Science user facility 352 under contract DE-AC05-00OR22725 operated by the Oak Ridge National Laboratory. This material is 353 based upon work supported by the Office of Basic Energy Sciences, U.S. Department of Energy. The authors wish to thank the ORNL committee for granting beam-time to the proposal IPTS-19146.1. Further, the authors wish to acknowledge the financial and technical support of Rolls-Royce plc.

References

1. L.N. Carter, M.M. Attallah, Superalloys 2012, Seven Springs, PA (2012).
2. S. Goutianos, IOP Conf Series- *Mat. Sci. Eng*, 219 (2017).
3. M. Krolikowski, K. Filipowicz, *Adv. In Manuf. Sci. Tech*, 37;3 (2013) pp95-91.
4. L. Carter, PhD Thesis, University of Birmingham (2013).
5. K. Harris, G.L. Erickson and R.E. Schwer, Superalloys 1984 Seven Springs PA, (1984).
6. L. Santodonato et al., Physics Procedia, 69; (2015) pp104-8.
7. I.S. Anderson *et al*, Neutron imaging & applications: Reference for the imaging community, Springer (2009).
8. I. Dhiman et al., *Review of Scientific Instruments*, 88;9 (2017) 095105.
9. Octopus Imaging, XRE NV, Technologiepark-Zwijnaarde 5, Gent, Belgium.
10. ThermoFisher Scientific, Hillsboro, Oregon 97124 USA.
11. P.A. Bagot et al, *Acta Materialia*, 125 (2016) pp156-165.
12. M. Rappaz, *Current Opinion in Solid State and Materials Science*, 20 (2016) 37-45.
13. R.C. Reed, The Superalloys: Fundamentals and Applications, Cambridge University Press (2006).
14. S.G. Protasova et al, J. *Mater. Sci*, 46, (2011) pp4349-4353
15. B.B. Straumal et al., *J. Mater*. Sci. 45, (2010) pp2057.

Figures and Tables

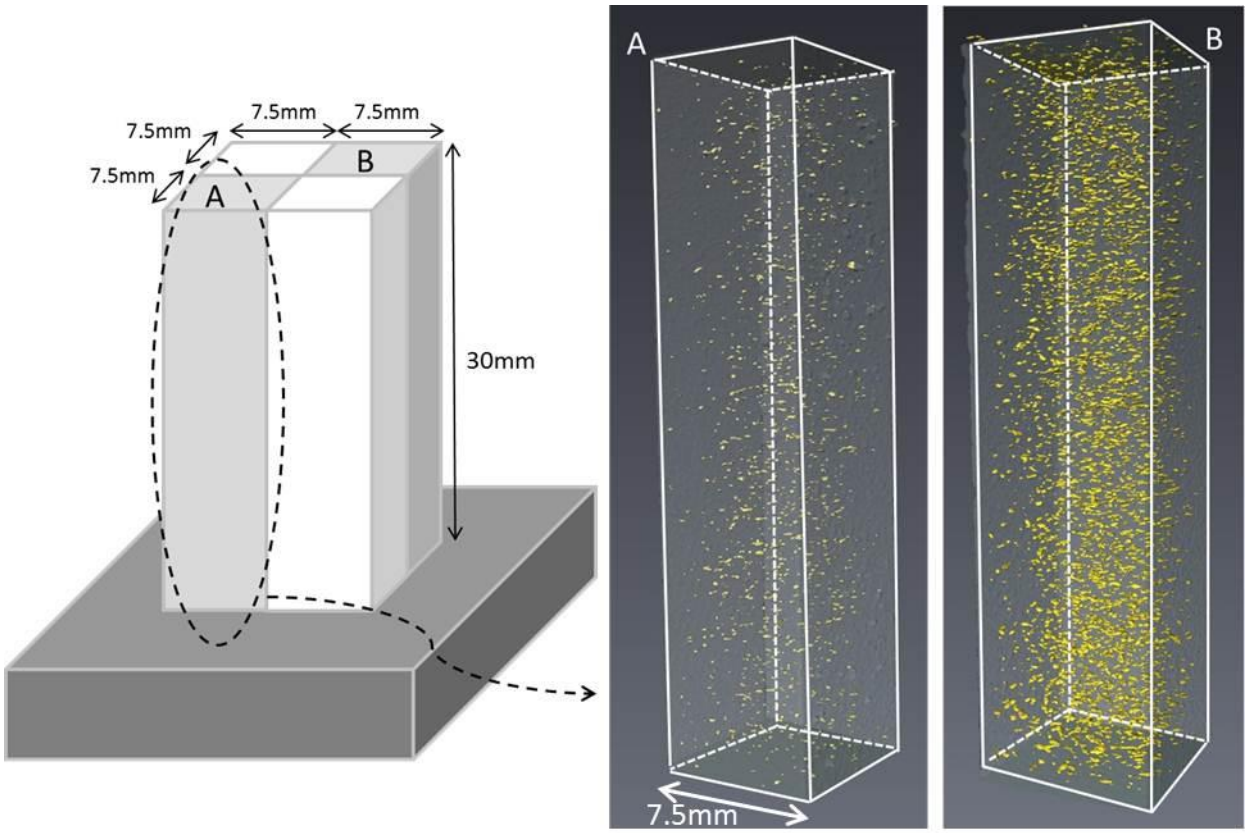

Figure 1: *Neutron tomography highlights significant variation in porosity measured in columns A and B cut from the same SLM-fabricated sample*

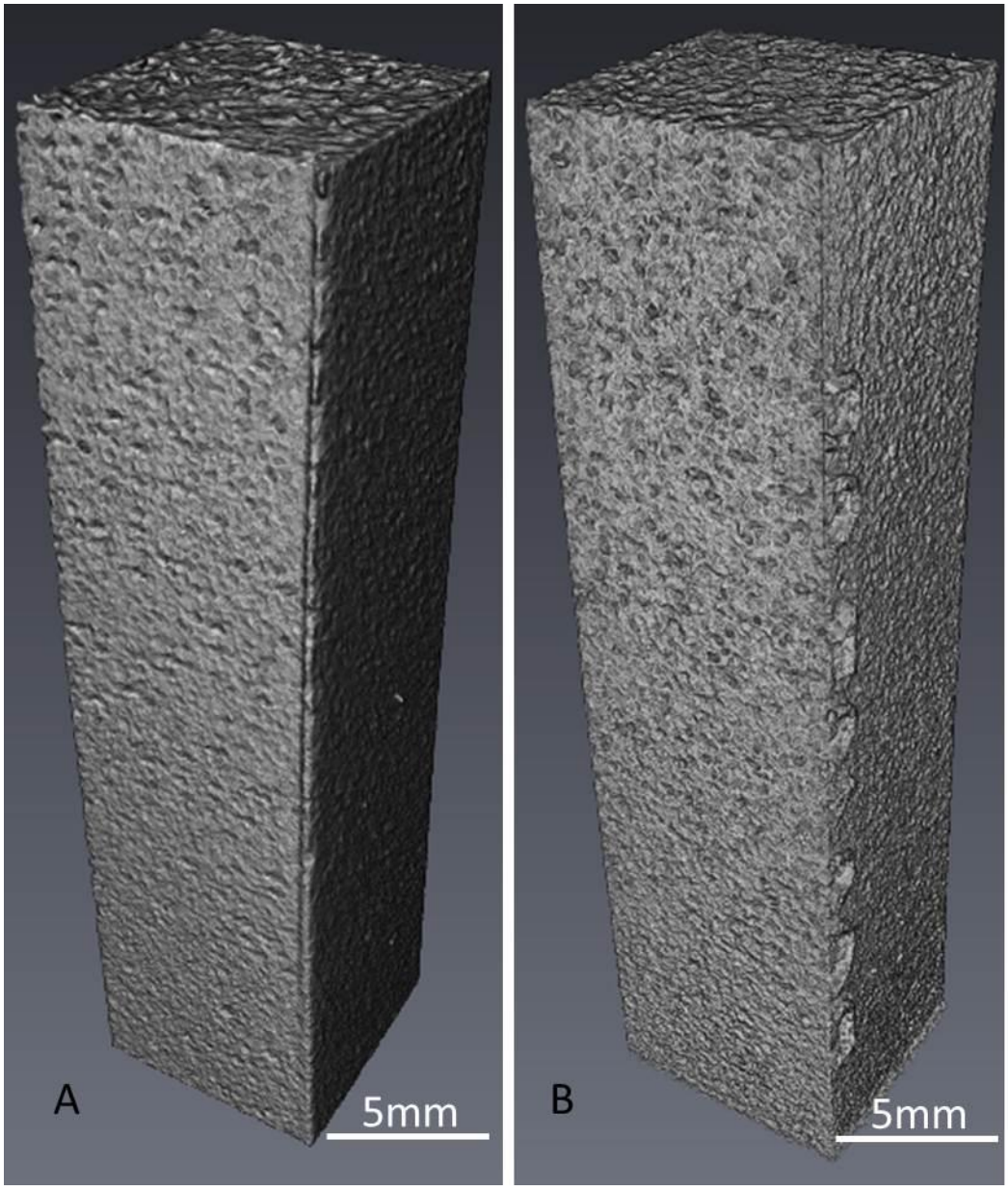

Figure 2: Avizo analysis of the SLM-fabricated neutron tomography data for sub-builds A and B, highlighting a potential grain boundary segregation effect shown as a network of lighter regions around grains.

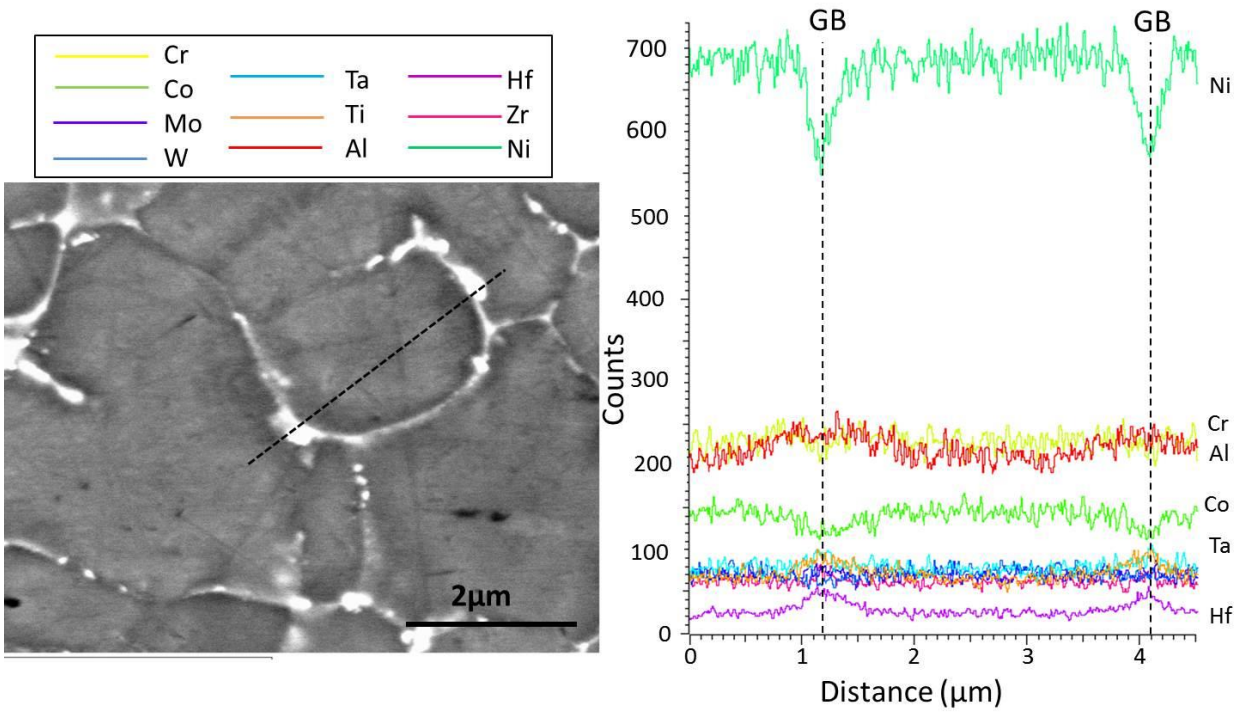

Figure 3: *EDX line-scan analysis of a region of the SLM build across a grain and grain boundary.*

Table 1*: EDX chemical composition of the CM247LC ALM build in the matrix and in the segregated material (at%)*

	Cr	Co	Mo	W	Ta	Ti	Al	Hf	Zr	Ni
Segregation	1.90	1.74	-	0.68	6.23	0.48	15.88	63.90	-	9.24
Grain	10.29	9.72	0.5	4.68	0.64	0.87	14.35	0.48	0.05	58.43